RESEARCH

Promoting epithelial regeneration in chemically induced acute lung injury through Sox9-positive alveolar type 2 epithelial cells

Chao Cao[1,2,3,6], Obulkasim Memete[1,2,3,6], Yu Dun[1,2,3,6], Lin Zhang[1,2,3], Fuli Liu[1,2,3], Daikun He[1,2,3], Jian Zhou[4,5,6], Yiru Shao[1,2,3*] and Jie Shen[1,2,3,6]

Abstract

Background Chemical-induced acute lung injury is characterized by impaired epithelial regenerative capacity, leading to acute pulmonary edema. Numerous studies have investigated the therapeutic potential of endogenous stem cells with particular emphasis on alveolar type 2 epithelial (AEC2) cells owing to their involvement in lung cell renewal. Sox9, a transcription factor known for its role in maintaining stem cell properties and guiding cell differentiation, marks a subset of AEC2 cells believed to contribute to epithelial repair. However, the role of Sox9+AEC2 cells in the distal lung alveolar cells and the potential roles in chemically induced acute lung injury have never been explored.

Methods In this study, we generated $Sox9^{flox/flox};Sftpc^{Cre-ERT2}$ mice and examined the effects of Sox9+AEC2 cells on the pathophysiology of epithelial damage during chemical-induced acute lung injury. Subsequently, $Sox9\text{-}Cre^{ERT2}$ ^{Ai9} mice were used for lineage tracing to elucidate the repair mechanisms.

Results Our findings revealed that Sox9+AEC2 cells endowed with stem cell properties induced cell proliferation during lung injury, predominantly in the damaged alveolar region. This process is accompanied by the regulation of inflammatory responses and orderly differentiation, thereby promoting epithelial regeneration.

Conclusion These results provide compelling in vivo genetic evidence supporting the characterization of Sox9+AEC2 cells as bona fide lung epithelial stem cells, demonstrating their multipotency and self-renewal capabilities during lung repair and regeneration. The identification of Sox9+AEC2 cells as crucial contributors to the promotion of epithelial repair underscores their potential as therapeutic targets in chemical-induced acute lung injury.

Keywords Alveolar type 2 epithelial cells, Sox9, Immune regulation, Cell differentiation, Epithelial regeneration, Chemically induced acute lung injury

*Correspondence:
Yiru Shao
shaoyiru1983@163.com
Full list of author information is available at the end of the article

Cao *et al. Stem Cell Research & Therapy*   (2025) 16:13

Page 2 of 18

Introduction
Background
Chemical-induced acute lung injury (CALI) is characterized by direct damage to the air-blood-barrier-alveolar epithelium a phenomenon that increases epithelial barrier permeability. This is followed by an exacerbated or uncontrolled inflammatory response, ultimately leading to a cascade of inflammatory changes in the lungs known as inflammatory storms [1, 2]. This poses a significant challenge for clinical treatment, and common causes include phosgene, diphenylene, chlorine, ammonia, and hydrofluoric acid. Phosgene is a crucial chemical raw material that is widely used in industrial production, including pesticides, plastics, dyes, polyurethane, and agrochemical synthesis. It is also indispensable for pharmaceutical production [3]. Accidental phosgene leakage is highly likely owing to improper production, transportation, or storage, leading to chemical injury accidents, especially acute lung injury induced in response to chemical exposure. The inhalation of toxic and harmful gases during such incidents can result in critically ill patients succumbing to improper treatment [4, 5]. Therefore, the development of new treatments aimed at reducing inflammation and promoting the regeneration of the alveolar epithelium and capillary endothelium is essential to attenuate lung damage and improve patient outcomes.

Understanding the role of lung-resident stem or progenitor cells in maintaining the epithelial barrier during lung homeostasis and repair could provide novel insights into therapeutic approaches for pulmonary diseases. Alveolar epithelial cells mainly consist of alveolar type 1 and 2 (AEC1 and AEC2) cells. Once damaged, these epithelial cells must be rapidly replaced to maintain lung structure and function [6, 7]. Alveolar epithelial regeneration is essential for recovery from lung diseases. This process occurs when AEC2 cells proliferate and transdifferentiate into AEC1 cells. More specifically, barrier injury to AEC2 cells has been linked to the pathogenesis of ALI [8], because AEC2 cells serve as facultative progenitors for the distal lung epithelium, a propensity for self-renewal, and regenerative potential upon reinjury [9]. Recent studies have focused on endogenous stem cells for the treatment of lung diseases, such as those involve the bronchioalveolar duct junction (BADJ) cells, which are more adept at sensing lung inflammation and regulating the microenvironment by promoting alveolar epithelial regeneration and repair or delaying pulmonary fibrosis [10]. However, the existence of functional stem cell subpopulations, especially their roles in epithelial repair, which is expected to reverse core pathological changes, remains controversial, and warrants further exploration.

Transcription factors play crucial roles in coordinating cell-specific gene networks that support pulmonary epithelial repair during ALI. The expression of these transcription factors is typically inhibited in fully developed adult lungs, thereby preventing cell overgrowth and lung dysfunction. Sex-determining region Y box 9 (SOX9) is a transcription factor that plays an essential role in mammalian development, particularly in the regulation of chondrogenesis and sex differentiation [11, 12]. Insights into Sox9 expression and function were primarily derived from studies on embryonic organ development, tracheal chondrogenesis, pulmonary branch morphogenesis, and male gonad development [13, 14]. Growing evidence suggests that SOX9 plays a regenerative role in pulmonary epithelial cells, indicating its potential in regulating cell proliferation during lung injury [15, 16]. Over the past decade, significant progress has been made in the identification of stem cells, and our previous studies utilizing single-cell transcriptomic analysis of lung cells have revealed that Sox9-positive AEC2 cells can serve as stem cells in adult lung tissue, providing novel insights for improving treatment efficacy [17]. Understanding the migration and nesting of stem cells at the site of injury is crucial to determine their repair function after tissue injury [18]. However, the potential mechanism and orderly differentiation of Sox9^{+}AEC2 cells in CALI and the signaling pathways still need to be elucidated.

Although the role of SOX9 in the epithelium during lung development is well documented, Sox9^{+}AEC2 cells in the distal alveolar cells of the lung and their potential role in repair have never been explored in the context of CALI. This study investigated the contribution of previously undefined cells expressing Sox9 in the AEC2 population to repair and regeneration in CALI. Our findings demonstrate that the increase in the number of Sox9^{+}AEC2 cells plays a pivotal role in pulmonary regeneration, highlighting the potential of these cells as a therapeutic target for CALI.

Methods
Mouse models
All animal experiments and conducted procedures were in accordance with the law on animal experimentation and are approved by the regulatory authorities. The work has been reported in line with the ARRIVE guidelines2.0.

C57BL/6 (wild type, WT), *Sox9^{flox/flox}*, and *Sftpc^{Cre−ERT2}* mice were obtained from Jiangsu Jinzhihe Biotechnology Laboratory, China. To generate epithelial cell type 2-specific Sox9-deficient mice, *Sox9^{flox/flox}* mice were bred with heterozygous *Sftpc^{Cre−ERT2}* mice, resulting in *Sox9^{flox/flox};Sftpc^{Cre−ERT2}* mice. *Sox9^{flox/flox};Sftpc^{Cre}* mice were used as controls. Mouse genotyping was performed via PCR using tail DNA. For lineage tracing, eight- to ten-week-old male *Sox9-Cre^{ERT2 Ai9}* mice were bred and euthanized after exposure to tamoxifen (Tam; Sigma, T5648-1G).

Cao *et al. Stem Cell Research & Therapy*   (2025) 16:13

Page 3 of 18

The amplified sequences were visualized by electrophoresis on a 1.5% agarose gel containing ethidium bromide. The forward and reverse primer sequences are listed in Supplementary Table 1 and 2. Mice were housed in a controlled environment under constant temperature and humidity (24–26 °C and 55–60% humidity), and subjected to a 12-h light and 12-h dark cycle with free access to food and water.

Mouse phosgene exposure experiments

Male mice aged between 8 and 10 weeks and weighing 20 ± 4 g were used in the animal studies. Intraperitoneal injections of Tam were administered at a dose of 100 mg/kg body weight daily for five consecutive days before exposure. CALI was induced by phosgene inhalation at the Animal Center of Fudan University, as described previously. Briefly, the mice in the control group were exposed to normal room air, whereas those in the phosgene group were exposed to 8.33 mg/L phosgene for 5 min in an airtight cabinet. Phosgene gas was produced by dripping N, N-dimethyl formamide (Macklin, Shanghai, China) into hexamethylene-containing triphosgene (Macklin). The mice were humanely euthanized using 100% carbon dioxide and decapitated within 5 min for tissue collection. Lung function parameters were collected and analyzed using histological, RNA, protein, and fluorescence immunoassays.

Hematoxylin and eosin (HE) staining

Lung specimens were collected, fixed overnight at 4 °C in 4% paraformaldehyde (Biosharp, BL539A), dehydrated, embedded in paraffin, and cut to a thickness of 5–8 µm using a microtome (Leica, Wetzlar, Germany). Paraffin sections of the lung tissue were stained in accordance with a standard protocol (Solarbio, G1120-100). The specimens were imaged under a light microscope (Nikon, Tokyo, Japan) and quantification was performed using a BZ-X analyzer. The cell counting method in the lung tissue has been outlined by Cheng et al. [19].

Lung injury score

The lung pathological injury was independently graded by two researchers according to previously described criteria [20].

RNA isolation and real-time PCR

RNA was extracted from lung tissues using TRIzol reagent (RR047A; Takara, Japan) following the instructions outlined in our previous study [17]. Subsequently, cDNA was synthesized and real-time PCR was conducted using the SYBR Green Premix Pro Taq HS qPCR Kit (cat. no. AG11701, Accurate Biology). Target gene transcripts were amplified from mice using the SuperScript III One-Step RT-PCR Kit (12,574,026; Thermo Fisher Scientific, Waltham, MA, USA) on a Roche LightCycler 480 platform. RT-PCR was performed on an Eppendorf Realplex 4 instrument (Eppendorf, Hamburg, Germany). Primer sequences for the target genes were obtained from Univ-Bio (Shanghai, China) and are provided in Supplementary Table 3. Relative gene expression was calculated using *Actb* as a reference. Results were expressed as the mean $\pm$ SD, with six biological replicates for each sample.

Immunohistochemistry and the IHC score

For immunological analyses, 8 µm microtome sections were deparaffinized for 30 min and rehydrated with gradient alcohol. Endogenous peroxidase activity was quenched using 3% H_2O_2, followed by heat-induced epitope retrieval. The sections were incubated overnight at 4 °C with primary antibodies targeting specific proteins (Supplementary Table 4). Specimens were washed three times with phosphate-buffered saline (PBS) before incubation with secondary antibodies for 30 min at 37 °C. A horseradish peroxidase conjugate was used for detecting the enzymatic assays. The IHC score was calculated by multiplying the percentage of positive cells with the staining intensity. The intensity was scored as 0 (negative), 1 + (weak staining), 2 + (moderate staining), or 3 + (strong staining) and the frequency was scored based on the proportion of positive cells.

(See figure on next page.)

Fig. 1 SOX9 is upregulated and mainly located around the alveolar region during in CALI. **A** WT mice were exposed with either air or phosgene for D3, D7 and D14. Immunoblotting was performed using antibodies against SOX9 and GAPDH. SOX9 protein levels were normalized to GAPDH and presented as fold induced change using a dot graph. **$P < 0.01$, ***$P < 0.001$; $n = 6$; Student's 2-tailed t test. Full-length blots were presented in Supplementary Fig. 6. **B** Quantification of Sox9 transcripts in total lung transcript RNA of the Control and Phosgene groups using real-time PCR (RT–PCR). ***$P < 0.001$; $n = 6$/group; Student's 2-tailed t test. **C** Immunostaining was performed with the anti-SOX9 antibody on alveoli sections of D3, D7, and D14 from normal healthy (Control) and Phosgene mice. Representative images were obtained at 40 × magnification. Scale bar: 100 µm. **D** Quantification of Sox9⁺AEC2 cells. **$P < 0.01$, ***$P < 0.001$, NS, not significant; $n = 6$/group; Student's 2-tailed t test. **E** and **F** Confocal microscopy images of lung section alveoli in Control and Phosgene stained with anti-SOX9 (red color), anti-SFTPC (green color) antibodies, and nuclei stained with DAPI (blue color). Quantification of Sox9⁺AEC2 cells. Cells positive for both SOX9 and SFTPC are highlighted with white arrows. Images obtained at 20 × magnification. Scale bar: 100 µm ($n = 6$/group). **$P < 0.01$, ***$P < 0.001$; $n = 6$/group; Student's 2-tailed t test
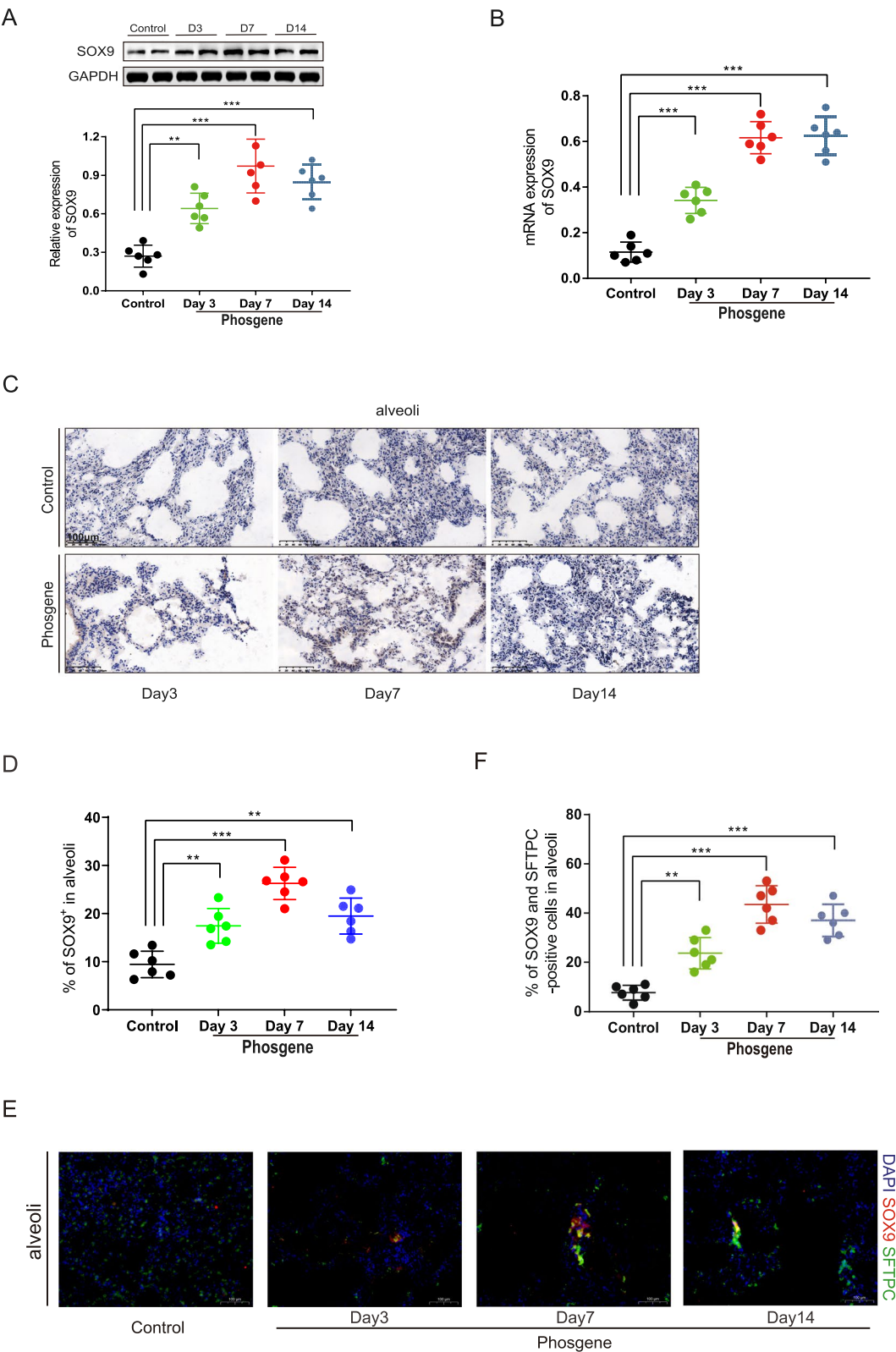
Cao *et al. Stem Cell Research & Therapy*   (2025) 16:13

Page 4 of 18

Fig. 1 (See legend on previous page.)

Cao *et al. Stem Cell Research & Therapy*   (2025) 16:13

Page 5 of 18

Immunofluorescence

Tissues pending inspection were fixed in 4% paraformaldehyde at 4 °C overnight and treated with Triton X-100 (Sigma, USA) permeabilization buffer. Following treatment, lung specimens were blocked with PBS containing 1% bovine serum and incubated with primary antibody at 4 °C. The samples were subsequently incubated with species-specific donkey Alexa Fluor 488, 568, or 647 antibodies (Supplementary Table 4) and stained with 4′,6-diamidino-2-phenylindole (DAPI). Images were captured using a laser scanning confocal microscope (Carl Zeiss AG, Oberkochen, Germany). Data were analyzed using Imaris or Elements software (Imaris 8.1; Oxford Instruments, Abingdon, United Kingdom).

Myeloperoxidase assay

Lungs were perfused with PBS to eliminate all blood, weighed, frozen, and stored at −80 °C before the assay. Myeloperoxidase (MPO) activity was measured as described previously [21].

Western blotting

Western blotting was conducted as per established procedures utilizing a protein extraction kit (Well-bio, Shanghai, China) according to the manufacturer's instructions [17]. The antibodies used for immunostaining and their dilutions are listed in Supplementary Table 4.

5-ethynyl-2′-deoxyuridine (EdU) incorporation analysis

Mice were treated with EdU (10 µmol/L) at the indicated times for 3 h. Staining was performed according to the manufacturer's instructions (Beyotime).

Enzyme-linked immunosorbent assay (ELISA)

Serum levels of TNF-α, IL-1β, IL-6, IL-12, and IL-4 were determined using a high sensitivity multiplex assay kit based on antibody immobilized fluorescently labeled microsphere beads. ELISA kits (LINCO Research, St. Charles, MO, USA) were used for the quantification. Cytokine concentrations were measured at 450 nm and calculated using linear regression analysis in GraphPad Prism 8.0.

Intratracheal cell infusion

A mouse model of CALI was established using phosgene exposure. Six hours after modeling, airway drip infusion was performed using WT-sorted AEC2 cells. For intratracheal dosing, all mice were deeply anesthetized with isoflurane in an induction chamber. $Sox9^{flox/flox};Sftpc^{Cre-ERT2}$ mice with pharmacologically induced Sox9 knockout were used as controls. Intratracheal cell administration was performed via a tracheal drip. The PBS solution, containing 2% mouse serum, was administered intratracheally to the WT and $Sox9^{-/-}$ groups. The solution was prepared with 5×10^5 WT-sorted AEC2 cells or $Sox9^{-/-}$ AEC2s. There were 6 mice in the WT and $Sox9^{-/-}$ groups. The detailed procedural steps have been outlined in our previous studies [20].

RNA-Seq and analysis

Cells from the bronchoalveolar lavage were loaded in phosphate buffered saline containing 0.05% bovine serum albumin according to the 10 × Genomics' protocol. The requisite preparation time for the cells prior to loading them onto the 10 × Chromium Controller in 2 h. Libraries were constructed using the Single Cell 3 Library Kit V2 (10 × Genomics, Pleasanton, CA, USA). Single cell transcriptome profiles were determined using 10 × Genomics-based droplet sequencing. Differential gene expression analysis was conducted on two groups using log2FoldChange values in RNA-seq analysis, with a significance threshold of p < 0.05. The results were presented visually using heatmaps and subjected to GSEA for enrichment analysis. The RNA-Seq data

(See figure on next page.)

Fig. 2 Sox9^{+}AEC2 cells exhibited proliferation and were predominantly concentrated in the alveolar region. **A** Confocal microscopy images of lung sections from Sham and CALI stained with anti-SOX9 (red color), anti-SFTPC (green color) antibodies, and nuclei stained with DAPI (blue color). Cells positive for both SOX9 and SFTPC are highlighted with white arrows. Images were acquired at 20 × or 60 × magnification. Scale bars: 100 µm (left), 20 µm (right). **B** Number of SOX-positive AEC2 (red and green color) cells in total cells (DAPI in blue color) quantified using the MetaMorph image analysis software and presented as the percentage of Sox9^{+}AEC2s in total epithelial cells. ***P < 0.001; n = 6; Student's 2-tailed *t* test. Representative coimmunostaining images showing Ki67 (green) and SOX9 (red) as markers for Sox9^{+}AEC2 proliferation in the alveoli region D3 and D7 after CALI (**C**) and quantification (**D**). Nuclei are shown with DAPI (blue). White arrows indicate exemplary Ki67^{+} SOX9^{+}AEC2s. Scale bars: 100 µm (left), 20 µm (right). A total of three lungs per group were stained, and six images per lung were analyzed for **D**. **P < 0.01, ***P < 0.001; n = 6; Student's 2-tailed *t* test. **E** Confocal images of lung sections from Sham and CALI mice stained with anti-SOX9 (red color), anti-PCNA (green color) antibodies, and nuclei stained with DAPI (blue color). Images obtained at 20 × or 60 × magnification. Scale bars: 100 µm (left), 20 µm (right). Scale bar: 50 µm (n = 6/group). **F** Percentage of PCNA[+] SOX9^{+}AEC2s in total cells. ***P < 0.001; n = 6; Student's 2-tailed *t* test. **G** Numbers of Sox9^{+}AEC2 (red and green color) cells, EdU-positive (orange color) cells, and total cells (DAPI or blue color). Representative confocal images were obtained at 20 × or 60 × magnification. Scale bars: 100 µm (left), 20 µm (right). **H** Images processes using the Elements image analysis software and presented as the percentage of EdU- Sox9^{+}AEC2 cells in total cells. **P < 0.01; n = 6/group; Student's 2-tailed *t* test
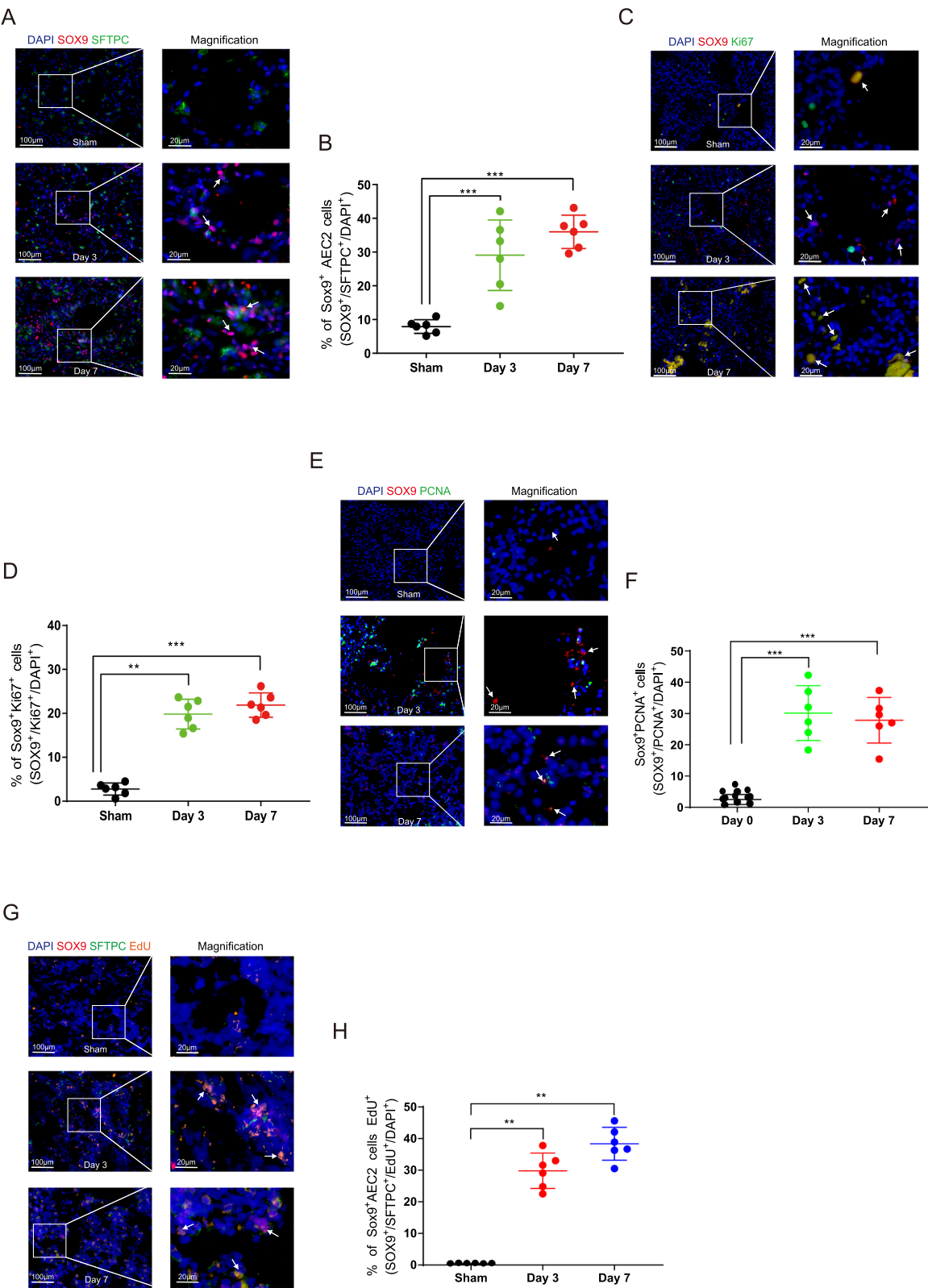
Cao *et al. Stem Cell Research & Therapy*   (2025) 16:13

Page 6 of 18

Fig. 2 (See legend on previous page.)

Cao *et al. Stem Cell Research & Therapy* (2025) 16:13

Page 7 of 18

were available at https://doi.org/https://doi.org/10.5061/dryad.dz08kps6w, and analyzed for protein interaction networks and pathways using STRING (https://cn.string-db.org/).

PI3K/AKT Pathway Inhibition

Perifosine (Beyotime, SC0227) was intraperitoneally administered to *Sox9-CreERT2 Ai9* mice once a week for 4 consecutive weeks at a dose of 250 mg/kg body weight to inhibit the PI3K/AKT pathway. Lung tissues were collected from each experimental group at a 72-h interval following the intervention. Subsequent analyses included HE staining, lung injury scoring, mRNA and protein detection, and immunofluorescence assessments. These procedures were performed in accordance with the methodology described in our previous study.

Statistics

Graphs and statistical calculations were generated using the Prism software version 8.0 (GraphPad). Statistical significance was determined using the tests specified in each figure legend. The numbers of experiments and animals analyzed are shown in each figure. The significance of the differences was evaluated using a two-tailed Student's t-tests or one-way analysis of variance. A *P*-value of < 0.05 was considered statistically significant. Unless otherwise indicated, dot graphs represent the mean ± SEM. All experiments were repeated a minimum of five times unless otherwise specified.

Results

SOX9 is upregulated and mainly located around the alveolar region in CALI

We analyzed the alterations in lung tissue injury and SOX9 expression in WT mice at various time points. Histopathological sections were used to assess the severity of tissue damage. The alveolar tissue appeared intact, exhibiting a thin and uniform thickness with no exudate present in the alveolar lumen, indicating the absence of lung injury (Supplementary Fig. 1A). In contrast, the histopathological observations of the phosgene-exposed group revealed varying degrees of injury. Interstitial lung edema, substantial erythrocyte exudates in the alveolar lumen, thickening of the alveolar wall with neutrophil infiltration, and alveolar collapse were evident, particularly on D7 and D14 (Supplementary Fig. 1B and C). These findings suggest that lung tissue damage, increased lung water content, and compromised permeability of the lung capillaries are consistent with the pathophysiological changes associated with acute lung injury. These changes served as markers to evaluate the stability of the CALI model. Further, they served as markers to evaluate the stability of the CALI model, demonstrating that the mouse model exposed to phosgene inhalation faithfully recapitulated the pathophysiological changes observed in acute lung injury.

Additionally, SOX9 was upregulated and primarily localized to the alveolar region during CALI, suggesting its potential involvement in response to lung tissue injury. Immunohistochemistry revealed a significant elevation in SOX9 expression within the bronchial sites and alveoli of the phosgene group at all observed time points during CALI (compared to that in the control group). The total protein levels of SOX9 isolated from phosgene-exposed lungs were significantly higher than the levels isolated from normal lungs, with the most pronounced elevation observed in the D7 group (Fig. 1A). Additionally, *Sox9* expression showed a clear increase compared to that in the control group, especially on D7 and D14 (Fig. 1B). This expression significantly increased with disease progression, reaching its peak on D7 (Fig. 1C, D). Co-immunostaining revealed a substantial increase in the number of cells double positive for SOX9 and SFTPC (SOX9+SFTPC+) in the alveoli of the phosgene group (Fig. 1E and F). Conversely, there was no significant change in the number of double-positive cells within the bronchial sites compared to the control group, with only a few scattered SOX9-labeled cells (Supplementary Fig. 1D and E). Collectively, these results highlighted that the proliferation of SOX9 and SFTPC double-positive cells was predominantly concentrated in the alveolar

(See figure on next page.)

Fig. 3 Sox9+AEC2 cells alleviate the severity of lung injury and improve prognosis during CALI. **A** Schematic showing experimental design. Timeline for tamoxifen and phosgene treatment, and time point analysis. **B** Illustration showing epithelial cell type 2-specific *Sox9*-deficient mice through generation of *Sox9flox/flox* mice were bred with heterozygous *SftpcCre−ERT2* or *SftpcCre2* mice. **C** Progressive weight loss after phosgene exposure in WT, *Sox9flox/flox*, *SftpcCre−ERT2* and *Sox9flox/flox*, and *SftpcCre* mice after 2 weeks ($n = 6$/group; Statistics obtained from 1-way ANOVA). **D** Representative images of H&E-stained lung sections from WT, *Sox9flox/flox*, *SftpcCre−ERT2* and *Sox9flox/flox*, and *SftpcCre* mice at different time points; 40×magnification, scale bar: 100 μm. Lung injury scores for each treatment group ($n = 4$–6/group). Lung injury score ($n = 6$–8/group, 2-way ANOVA), **E** Ratios of wet to dry lung weight ($n = 5$–6/group). **F** Quantitative analysis of neutrophil infiltration by measurement of lung tissue MPO activity ($n = 5$/group). **G** Quantitative analysis for leukocyte infiltration in lungs ($n = 5$–6/group). Results are shown as mean ± SEM. Statistics obtained from 1-way ANOVA. **$P < 0.01$, ***$P < 0.001$, WT vs. *Sox9flox/flox*, *SftpcCre−ERT2* groups; #$P < 0.05$, ##$P < 0.01$, ###$P < 0.001$, *Sox9flox/flox*, *SftpcCre−ERT2* vs. *Sox9flox/flox*, *SftpcCre*; NS, no significant
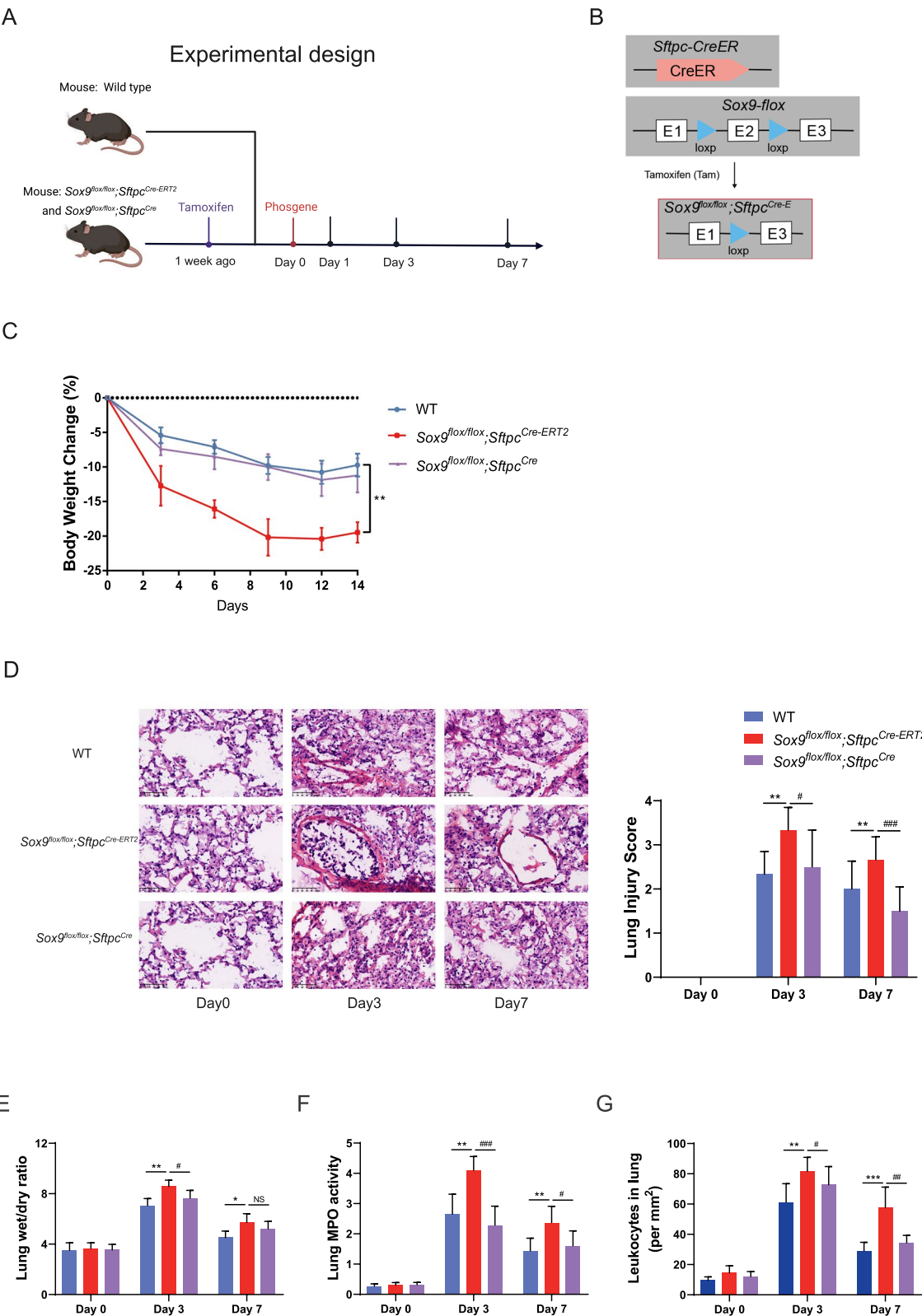
Fig. 3 (See legend on previous page.)

region. This observation provides additional confirmation that this cell subpopulation corresponds to SOX9-positive alveolar type 2 epithelial (AEC2) cells.

Sox9⁺AEC2 cells exhibited proliferation and were predominantly concentrated in the alveolar region

Following CALI, repair activities are prominently centered in the damaged alveolar region, particularly during post-injury initiation of the epithelial tissue repair process. Consequently, our focus was directed toward examining functional changes in Sox9⁺AEC2 cells on D3 and D7 in the alveolar region in this section, along with immunofluorescence. Co-immunostaining revealed an augmentation in cells double-positive for SFTPC and SOX9 within the alveolar lesions of the D3 and D7 groups, indicating a significant increase in the number of Sox9⁺AEC2 cells at these two time points (compared to the normal state) (Fig. 2A, B). Subsequently, we utilized the expression of Ki67 and PCNA to assess the proliferation of Sox9⁺AEC2 cells. The results demonstrated a significant increase in the number of Sox9-positive cells in the D3 and D7 groups (Fig. 2C–F), suggesting robust proliferation of Sox9-positive cells. Notably, the Sox9⁺AEC2 cell population exhibited a clear increase on D3 and D7 post-injury.

5-Ethynyl-2′-deoxyuridine is widely used in the research on DNA damage repair, virus propagation, and cell proliferation, differentiation, growth, and development. We examined the proliferation of Sox9⁺AEC2 cells at different stages by probing them with SOX9 and SFTPC. The results showed substantial cell proliferation in the D3 and D7 groups compared to that in the sham group (Fig. 2G, H), with a marked increase in cell count. This finding further confirms that Sox9⁺AEC2 cells undergo significant proliferation during CALI, and are concentrated in the alveolar region, with an elevated cell population. These conditions are crucial to facilitate the repair of lung injury.

Sox9⁺AEC2 cells play a protective role in epithelial repair and mitigating inflammatory responses during CALI

We generated conditioned knockout mice with *Sox9* selectively deleted from alveolar type 2 epithelial cells to elucidate the impact of Sox9⁺AEC2 cells on lung repair following CALI. The mice were subsequently exposed to phosgene (Fig. 3A). Transgenic mice were generated based on the genotyping results (Fig. 3B). Specifically, *Sox9^{flox/flox}; Sftpc^{Cre−ERT2}* and *Sox9^{flox/flox}; Sftpc^{Cre}* mice were chosen, and the validation results are presented in Supplementary Fig. 2A. In *Sox9^{flox/flox}; Sftpc^{Cre−ERT2}* mice, SOX9 protein disappeared after Tam intervention, while alveolar type 2 epithelial cells were still distributed around the alveoli (Supplementary Fig. 2B). Deletion of Sox9⁺AEC2s resulted in a significant decrease in mouse body weight (Fig. 3C), and this impairment included reduced fluid exudation, tissue edema, inflammatory cell infiltration, and restoration of normal lung structure (Fig. 3D-F). Furthermore, the infiltration of neutrophils into the lungs significantly increased in *Sox9^{flox/flox}; Sftpc^{Cre−ERT2}* mice exposed to phosgene compared to both *Sox9^{flox/flox}; Sftpc^{Cre}* and WT mice treated with phosgene (Fig. 3G).

Exposure to phosgene resulted in increased levels of pro-inflammatory cytokines (TNF-α, IL-1β) and IL-6 and IL-12 (p70) in the serum (Fig. 4A–D). Notably, the levels of these pro-inflammatory factors were significantly elevated in the *Sox9^{flox/flox}; Sftpc^{Cre−ERT2}* group compared to those in the other two groups. The expression of the anti-inflammatory factor IL-4 also significantly increased to varying degrees on D1, D3, and D7 in each group. However, dynamic observations revealed a significant increase in the *Sox9^{flox/flox}; Sftpc^{Cre−ERT2}* group (Fig. 4E).

Intratracheal drip therapy provides the advantage of directly targeting the lesion; therefore, we further investigated the therapeutic impact of Sox9⁺AEC2 cells. SOX9 is predominantly localized in the nuclei of spindle cells in distal alveolar lesions during lung injury [22], a phenomenon that was confirmed in Supplementary Fig. 1D and E. We subsequently employed a strategy involving the tracheal drip injection of AEC2 cells isolated from WT

(See figure on next page.)

Fig. 4 Sox9⁺AEC2 cells play a protective role in epithelial repair and the mitigation of inflammatory responses during CALI. Inflammatory cytokine analysis and inflammatory response evaluation of WT, *Sox9^{flox/flox}, Sftpc^{Cre−ERT2}* and *Sox9^{flox/flox}*, and *Sftpc^{Cre}* mice on D0, D1, D3, and D7 after CALI by inhalation of phosgene. **A**–**E** Circulating concentrations of pro-inflammatory cytokines, including TNF-α (**A**), IL-1β (**B**), IL-6 (**C**), and IL-12(p70) (**D**), and anti-inflammatory cytokine levels of IL −4 (**E**) in serum of WT, *Sox9^{flox/flox}, Sftpc^{Cre−ERT2}* and *Sox9^{flox/flox}*, and *Sftpc^{Cre}* mice serum measured by ELISA ($n = 4$–6/group). Statistics obtained from 1-way ANOVA. The intratracheal drip injection of cells containing Sox9⁺AEC2 significantly attenuated phosgene-induced chemical lung injury. *$P < 0.05$, **$P < 0.01$, ***$P < 0.001$, WT vs. *Sox9^{flox/flox}, Sftpc^{Cre−ERT2}* groups; ##$P < 0.01$, ###$P < 0.001$, *Sox9^{flox/flox}, Sftpc^{Cre−ERT2}* vs. *Sox9^{flox/flox}, Sftpc^{Cre}*. NS, no significant. **F** Hematoxylin and eosin (H&E) staining was performed to observe histological changes in the lungs of each group (40×magnification). **G** Lung injury scores were significantly reduced at 24 and 48 h after the drip injection of phosgene-injured cells. **H** ELISA was conducted to measure the levels of the inflammatory factors TNF-α, IL-1β, and IL-4 in bronchoalveolar lavage fluid at different time points. *$P < 0.05$, NS, not significant; $n = 6$/group, as determined by unpaired Student's t-test
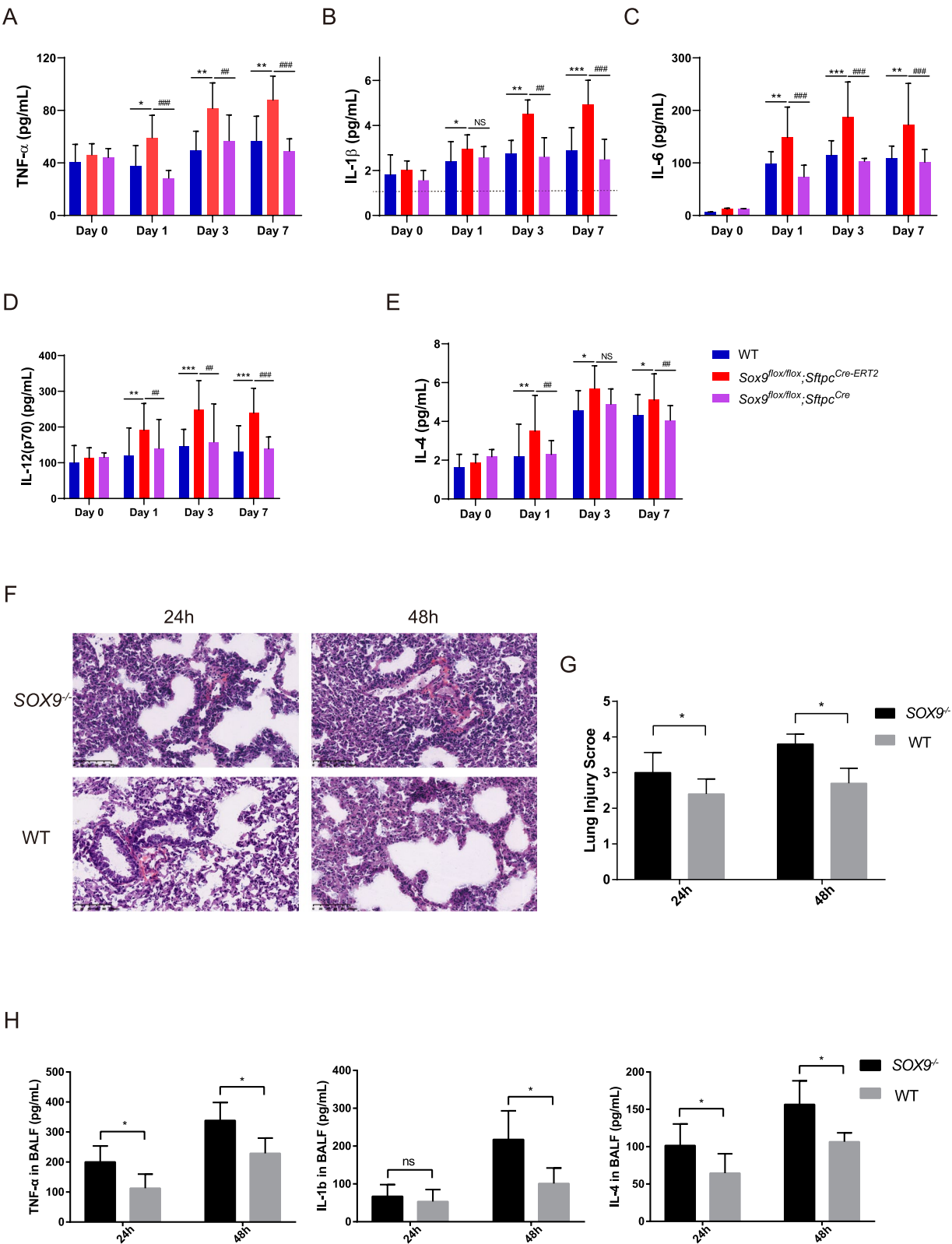
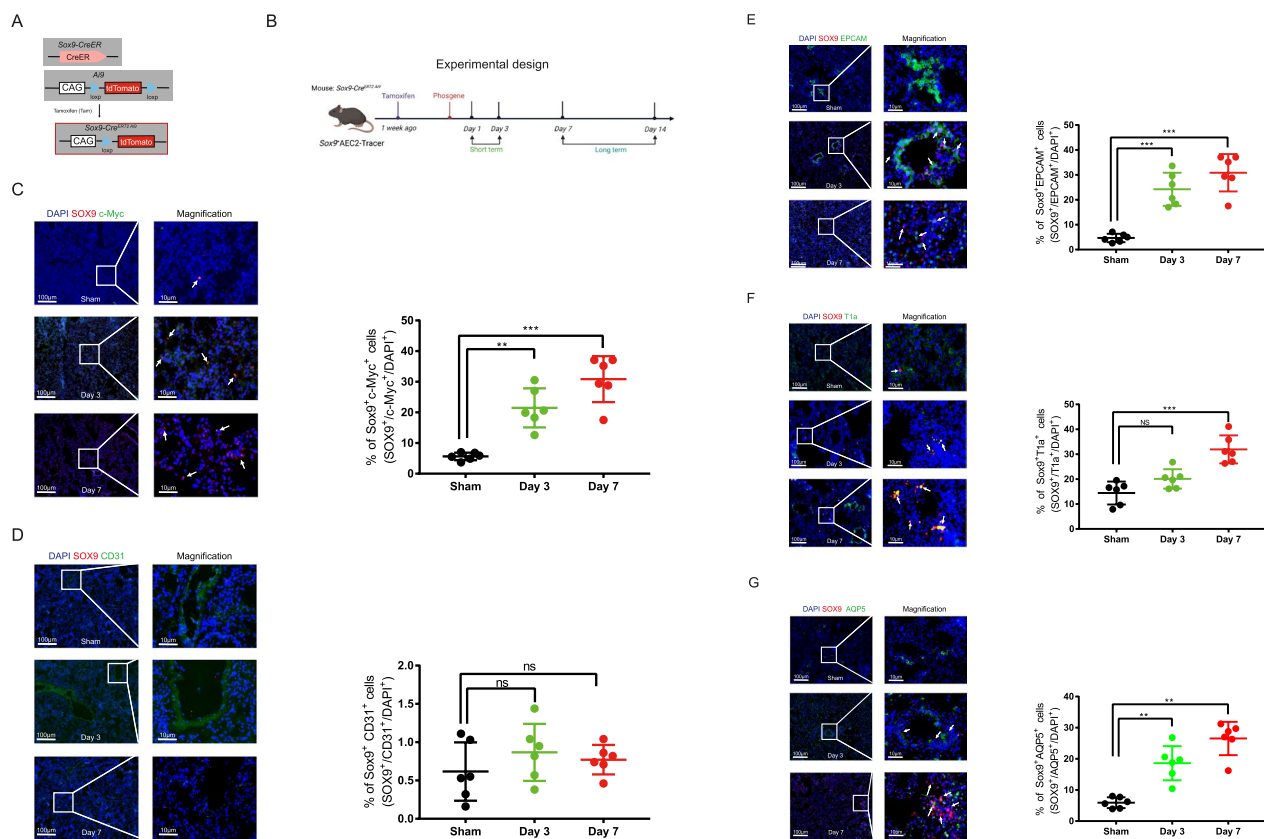**Fig. 4** (See legend on previous page.)

Fig. 5 Sox9+AEC2 cells promote epithelial repair through ordered differentiation. **A** Illustration of an intersectional genetic lineage-tracing strategy for Sox9+AEC2 cells, using a *Sox9-CreERT2 Ai9* mouse. **B** Schematic showing experimental design. Samples were analyzed after short-term or long-term tracing. **C** Immunostaining for SOX9 (red color), c-Myc (green color), and nuclei stained with DAPI (blue color) on lung tissue sections, and quantification of the percentage in each alveoli field. White arrowheads indicate SOX9+ c-Myc+ cells (*n* = 6/group). **D** Immunostaining for fluorescent proteins SOX9 and CD31 on lung sections and quantification of the percentage in each alveoli region (*n* = 6/group). **E** Confocal microscopy images of lung sections stained with SOX9 and EPCAM on lung sections and quantification of the percentage in each staining. Cells positive for both Sox9 and Epcam are highlighted with white arrows (*n* = 5–6/group). **F** Representative images of SOX9 and T1a on lung sections and quantification of the percentage in each alveoli field. White arrowheads indicate Sox9+ AEC1s differentiated from Sox9.+AEC2s (*n* = 5–6/group). **G** Immunostaining for fluorescent proteins SOX9 and AQP5 on lung sections and quantification of the percentage in each alveoli field. **P < 0.01, ***P < 0.001, NS, not significant, *n* = 5–6; *P* values were calculated with 1-way ANOVA. Each image is representative of three biologically independent mice. Representative confocal images were obtained at 20× or 100× magnification. Scale bars: 100 μm (left), 10 μm (right)

and *Sox9flox/flox;SftpcCre−ERT2* mice, where Sox9+AEC2 cells were removed. An intratracheal injection 1 h after CALI modeling was used for comparison. The *Sox9−/−* group exhibited significantly increased inflammatory cell infiltration and hemorrhage in the lung tissue at 24 and 48 h (Fig. 4F). Furthermore, the WT group demonstrated significantly lower lung injury scores (Fig. 4G), and the alveolar lavage fluid showed significantly lower levels of inflammatory factors (TNF-α, IL-6, and IL-4) (Fig. 4H). Taken together, these findings suggest that the subpopulation of epithelial cells containing Sox9+AEC2 cells has a substantial ameliorating effect on tissue injury and the inflammatory response during CALI.

Sox9+AEC2 cells promote epithelial repair through ordered differentiation

Given the pivotal role of Sox9+AEC2 in lung structural recovery, we investigated the underlying repair mechanisms. To achieve this, we established *Sox9CreERT2 Ai9* mice as a genetic lineage-tracing system specifically designed for the in vivo tracking of tamoxifen-induced Ai9 expression, facilitating the targeted tracing of *Sox9*-expressing cells (Fig. 5A, Supplementary Fig. 3A). Lineage tracing confirmed that most of the Sox9-expressing cells were marked after induction (Supplementary Fig. 3B). As expected, we observed a significant increase in the percentage of Sftpc+SOX9+ cells (Sox9+AEC2 cells) and Sox9+Ki67+ cells (proliferating cells) in the lungs of phosgene-stimulated *Sox9CreERT2 Ai9* mice, and Ai9+ cells expanded after 3 days (Supplementary Fig. 3C, D).

We subsequently traced the fate of Sox9$^+$AEC2 cells during lung regeneration by collecting *Sox9$^{CreERT2\ Ai9}$* mouse lungs at 1 and 3 days (short-term) and 7 and 14 days (long-term) after tamoxifen treatment (Fig. 5B). We expanded our investigation to the surrounding alveolar region by capitalizing on their stem cell properties and observing the proliferation and recruitment of Sox9$^+$AEC2 cells to the damaged alveolar region. Our findings revealed a notable increase in the proportion of cells dual-labelled with Sox9 and c-Myc in groups D3 and D7, indicating that the Sox9$^+$AEC2 subpopulation does possess stem cell properties (Fig. 5C). Despite lung injury manifesting as epithelial barrier and vascular endothelial damage, lineage tracing analysis demonstrated that the number of SOX9$^+$CD31$^+$ dual-labeled cells did not exhibit significant changes (Fig. 5D). This confirmed that Sox9$^+$AEC2 cells underwent limited differentiation into endothelial cells during lung injury.

Studies on epithelial cell differentiation demonstrated a substantial increase in the number of SOX9- and EpCAM-positive cells in the D3 and D7 groups, which were predominantly concentrated in the alveolar region (Fig. 5E). This further substantiated the ability of Sox9$^+$AEC2 cells to differentiate into epithelial cells. Subsequently, we analyzed the differentiation trajectory towards type 1 epithelial cells, utilizing specific markers T1α and aquaporin 5 (AQP5) in conjunction with autofluorescent SOX9 to track the cell differentiation path. The proportions of T1α$^+$SOX9$^+$ and AQP5$^+$SOX9$^+$ cells exhibited a significant proliferation in the D7 group compared to the Sham group, while changes were not statistically significant in the D3 group (Fig. 5F, G). This could be attributed to the fact that epithelial tissue repair requires a certain amount of time after lung injury. Sox9$^+$AEC2 cells contribute to restoration of the epithelial barrier through organized differentiation into epithelial cells (particularly AEC1 cells) during CALI. These findings provide compelling evidence for in vivo cell differentiation, supporting the assertion that Sox9$^+$AEC2 cells indeed belong to the category of epithelial stem cells and differentiate into AEC1 cells during the repair and regeneration processes following lung injury. Overall, these findings suggest that Sox9$^+$AEC2 cells proliferate

and ultimately differentiate into AEC1 cells during CALI, a phenomenon that contributes to alveolar regeneration.

The maintenance of stem cell regenerative ability by Sox9$^+$AEC2 cells is facilitated by activating the PI3K/AKT pathway

Single-cell RNA-seq was conducted on fluorescence assisted cell sorting (FACS)-purified lineage-labeled epithelial cells isolated from all subpopulations of the bronchoalveolar lavage fluid following phosgene challenge. We initially assessed Sox9 expression in cycling basal keratinocytes, which play a role in lung epithelial regeneration (Fig. 6A). Following data integration, we annotated the epithelial clusters using previously reported and validated marker genes (Supplementary Fig. 4A) and UMAP plot analyses (Fig. 6B, Supplementary Fig. 4B). These results indicated a close association between Sox9 and the PI3K/AKT signaling pathway. Sox9$^+$ cells effectively maintained the regenerative capacity of stem cells by activating the PI3K/AKT pathway (Fig. 6C-E, Supplementary Fig. 5A). This discovery supports further exploration of the molecular mechanisms and biological effects of these cells (Supplementary Fig. 5B). Downstream targets of the PI3K-AKT pathway, including PDK1, GSK3, SGK, and mTOR, were significantly upregulated, whereas FOXO, BAD, and PTEN were downregulated (Fig. 6F), indicating activation of the PI3K/AKT signaling pathway (Fig. 6G).

We used a specific AKT inhibitor (perifosine) to explore its reparative function and investigate the involvement of the PI3K-AKT signaling pathway in epithelial repair facilitated by Sox9$^+$AEC2 cells during CALI. A notable decrease in AKT mRNA expression was observed following inhibitor administration (Fig. 7A), and protein blotting analysis confirmed a significant reduction in AKT protein levels (Fig. 7B). Histological examination of lung tissues revealed thickened alveolar septa and an exacerbated degree of lung injury after perifosine intervention, as illustrated by HE staining (Fig. 7C). Furthermore, fluorescence staining in combination with EdU revealed a significant decrease in Sox9$^+$AEC2 cell proliferation in the alveolar region after AKT inhibitor blockade (Fig. 7D). Additionally, lineage-tracing results demonstrated that Sox9-expressing cells

(See figure on next page.)

Fig. 6 Sox9$^+$AEC2 cells maintain the regenerative ability of stem cells via the AKT/PI3K pathway. **A** Dot plot showing the pattern of *Sox9* expression of epithelial cells for the cell cluster on the UMAP map. **B** UMAP plots of the cell-type distribution of all identified epithelial cells, including Sox9$^+$AT, AT, Cillated, Club, and Fibroblast cells. **C** Enrichment of different KEGG pathways identified in the Sox9$^+$AECs cell population in the scRNA-Seq data. **D** UMAP map showing the pattern of the PI3K/AKT pathway for the cell clusters. **E** Protein interaction network among genes presented. **F** Volcano plot analysis of gene changes, including PDK1, SGK, GSK3, mTOR, PTEN, BAD, and FOXO. **G** KEGG pathway and GO analysis of PI3K and other related genes
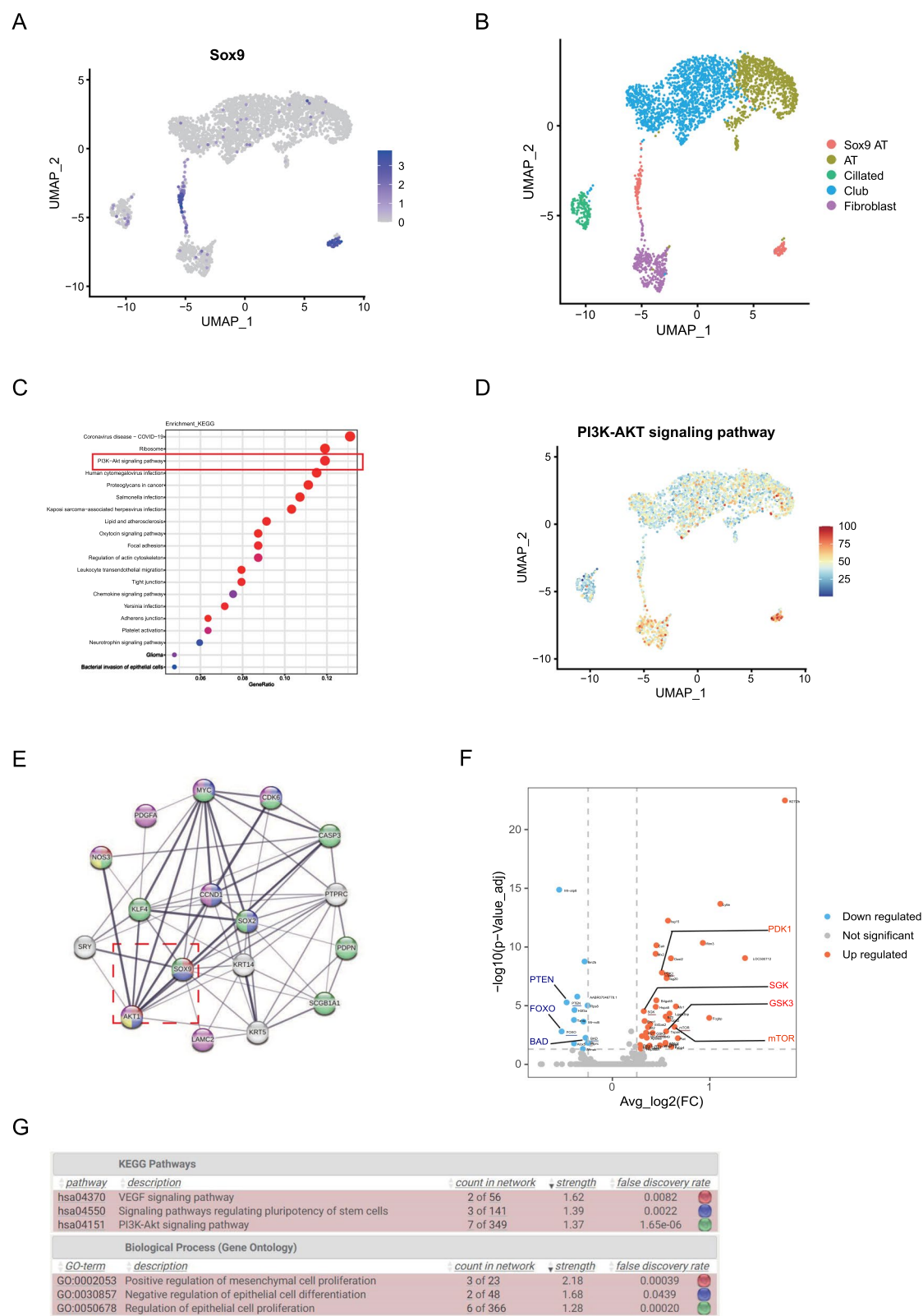
Fig. 6 (See legend on previous page.)

Cao *et al. Stem Cell Research & Therapy*   (2025) 16:13

Page 14 of 18

were unable to differentiate into functional cells compared to the control group cells (Fig. 7E). Collectively, these findings suggest that the regeneration and repair capabilities of Sox9^{+}AEC2 cells in CALI are intricately regulated by the PI3K/AKT pathway. Notably, inhibiting PI3K/AKT pathway diminished the protective effect of Sox9^{+}AEC2 cells against chemical lung injury.

Discussion

Stem cells are characterized by their multidirectional differentiation potential, self-replicating ability, and immunomodulatory capabilities and play a crucial role in the early stages of lung injury [23]. Strategies focusing on reducing inflammatory damage and enhancing alveolar epithelial regeneration are pivotal for promoting lung repair in CALI [24]. Endogenous stem cells possess unique properties and are emerging as novel therapeutic targets. The results of our study highlight that Sox9^{+}AEC2 cells play a protective role during CALI and contribute to tissue repair by regulating the immune microenvironment, influencing cell differentiation, and promoting tissue regeneration. Sox9^{+}AEC2 cells undergo differentiation post-injury, primarily transforming into AEC1 cells rather than into endothelial cells. The peak of this differentiation process was observed on D7, supporting the results obtained from the temporal analysis using single-cell sequencing. Moreover, elucidating the single-cell transcriptional profiles of lung immune cells identified cell-specific transcriptional profiles that affect the proliferation and differentiation of Sox9^{+}AEC2 cells by influencing the PI3K/AKT pathway, which is an essential player in the tissue regeneration and repair process in CALI.

Stem cell studies have uncovered distinct molecular markers for identifying cells with regenerative potential [25]. Among these markers, Sox9 (a member of the SRY-box-containing (SOX) protein family) stands out as a biomarker exhibiting stem cell attributes, confirmed through lineage tracing in various organs [17, 26, 27]. In addition to cholinergic anti-inflammatory effects, evidence supports the involvement of Sox9 in regulating the proliferation [28], differentiation [29], and cell migration capacity [30] of stem cells and their stem cell niche[17] in different organs. Notably, Sox9 plays a pivotal role in hair growth and development by guiding the differentiation of outer root sheath cells and promoting the formation of hair stem cell compartments under specific conditions [31]. Furthermore, extensive research has elucidated the function and mechanism of action of Sox9 in lungs [32]. However, its expression appears to be downregulated with alveolarization, and Sox9 is rarely expressed in the epithelial or mesenchymal cells of the adult distal lung [13, 33].

In our previous study, single-cell sequencing identified a distinct subpopulation of endogenous Sox9^{+}AEC2 cells recruited to the alveolar region in response to lung injury, which significantly ameliorated the extent of injury. The expression of both Sox9 mRNA and protein was significantly elevated in the affected lung tissues. Classical proliferative markers Ki67 and PCNA confirmed the proliferation of Sox9^{+}AEC2 cells, which were predominantly concentrated in the alveolar regions, thereby providing the necessary conditions for epithelial repair. Furthermore, the severity of lung injury significantly increased following the conditional knockdown of Sox9 in AEC2s. The levels of inflammatory factors, including pro-inflammatory and anti-inflammatory factors were substantially elevated, accompanied by intensified lung tissue infiltration. Conversely, tracheal drip infusion of Sox9^{+}AEC2 cells significantly attenuated inflammatory cell infiltration and lung tissue hemorrhage. The lung injury score was markedly reduced, and the levels of inflammatory factors in the alveolar lavage (TNF-α, IL-6, and IL-4) were significantly diminished. This underscores the substantial ameliorative effects of Sox9^{+}AEC2 cells on CALI.

The therapeutic potential of stem cells in lung injury depends on their capacity for multidirectional differentiation and immunomodulatory effects [9, 34–36]. A prominent pathological feature of CALI is the disruption of alveolar epithelial integrity. Repairing the integrity of the epithelial barrier is a pivotal step in treating lung injury to preventing inflammatory cell leakage and facilitating

(See figure on next page.)

Fig. 7 AKT/PI3K pathway inhibitor attenuates the protective effect of Sox9^{+}AEC2 cells during CALI. AKT inhibitor (perifosine) was intragastrically administered after CALI damage. Lung tissues were collected on D3, D7, and D14 after phosgene exposure. **A** Quantification of Sox9 transcripts in primary lung epithelial grown from control and perifosine lungs by qPCR. **B** Immunoblot analyses showing AKT and p-AKT (Ser473) changes in the Control and Perifosine groups. Full-length blots were presented in Supplementary Fig. 6. Data were presented as mean ± SEM. **C** Representative images of H&E-stained lung tissue from Control and Perifosine mice after CALI. Lung injury scores for each treatment group. **D** Representative confocal images and quantification, showing Sox9^{+}AEC2s proliferation in response to AKT inhibitor and phosgene stimulation. Scale bar: 20 µm, *n* = 3 mice per group with a total 18 random fields for quantification. **E** Immunostaining for SOX9 and AQP5 on lung sections after perifosine or vehicle treatment. White arrowheads indicate AEC1 cells derived from Sox9^{+}AEC2s. Quantification of the SOX9^{+}AQP5^{+} cell number in each alveoli field. Scale bar: 20 µm, *n* = 3 mice per group with a total 18 random fields for quantification. *$P < 0.05$, **$P < 0.01$, NS, not significant; *n* = 5–6/group; 1-way ANOVA
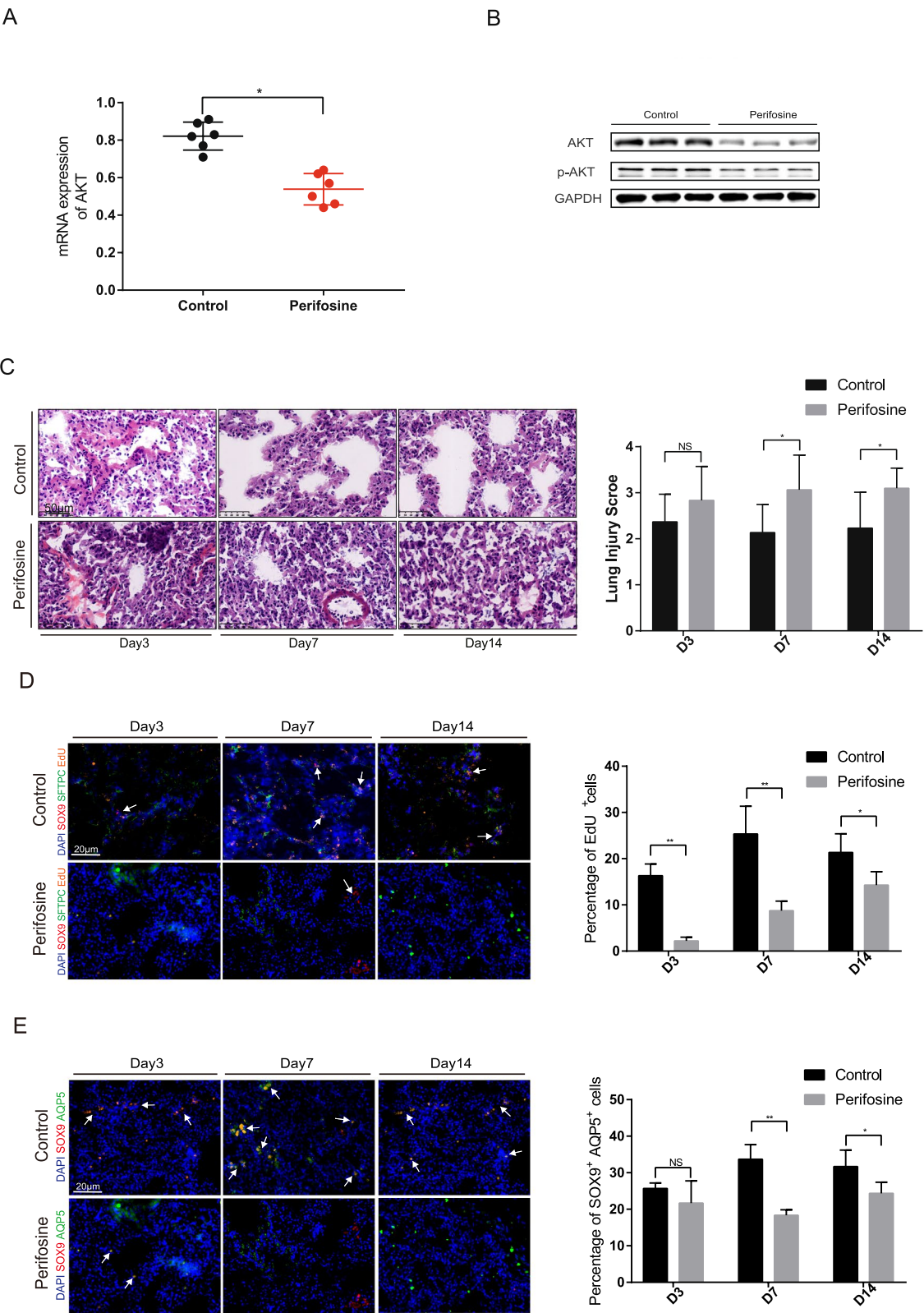
Cao *et al. Stem Cell Research & Therapy*   *(2025) 16:13*

Page 15 of 18

Fig. 7 (See legend on previous page.)

Cao *et al. Stem Cell Research & Therapy*   (2025) 16:13

Page 16 of 18

gas exchange. The proliferation of the Sox9^{+}AEC2 subpopulation after injury serves as a foundation for epithelial repair. Tissue repair requires the migration or homing of stem cells to the injury site [37, 38]. Previous studies established a significant role for Sox9 in alveolar epithelial cell regeneration, suggesting its potential to regulate cell proliferation after lung injury [39–41]. Various growth factors can upregulate Sox9 in fibroblasts and epithelial cells. Significant proliferation of Sox9^{+}AEC2 cells was observed in CALI, and their migration to the damaged alveolar region was identified as a crucial basis for alveolar epithelial repair. Notably, expression of c-Myc (a major transcription factor involved in cell proliferation and a stem cell marker) further corroborates the stem cell characteristics of this subpopulation. Analysis of tissue sections from various regions at different time points, combined with other cell type-specific markers, revealed that Sox9^{+}AEC2 cells underwent differentiation after injury, primarily differentiating into type 1 epithelial cells rather than endothelial cells. The peak of differentiation was observed on D7, consistent with the proposed time-series analysis by single-cell sequencing and aligned with the characteristic tissue repair features of CALI.

Subsequently, we investigated the specific mechanisms by which Sox9^{+}AEC2 cells participate in tissue repair using scRNA-Seq data. Notably, the genes upregulated in Sox9^{+}AEC2 cells were significantly enriched in the PI3K/AKT pathway, which is frequently implicated in cancer [42, 43]. Earlier studies indicated that inhibition of the PI3K/AKT pathway leads to decreased DNA repair [44, 45], resulting in increased apoptosis in lung injury. Conversely, other studies have highlighted the protective and regenerative functions of PI3K/AKT-dependent pathways after lung injury [46]. Recent cell signaling studies revealed that Sox9 can activate the PI3K/AKT pathway and promote cell proliferation, indicating a potential role for Sox9 in regeneration and repair [47, 48]. Our study further validated these findings using in vivo AKT inhibitor assays, demonstrating that interference with the PI3K/AKT pathway could affect cell proliferation, hinder the ability of Sox9-expressing cells to differentiate into AEC1 cells, and diminish the protective role of Sox9^{+}AEC2 cells in lung injury. However, given the pivotal role of the PI3K/AKT pathway in immune cell function, perifosine may exert an influence on neutrophil or monocyte/macrophage activity. Therefore, further study should be carried out to explore the potential benefits and risks.

This study has certain limitations. While we successfully confirmed the stem cell properties of Sox9^{+}AEC2 cells and demonstrated their efficacy in repairing the epithelial barrier in an animal model, our experiments were limited to male mice, which may not fully capture sex-specific responses. Additionally, while the animal model provides valuable insights, species-specific differences could impact the applicability of our findings to human subjects. Further experiments are essential to ascertain the potential therapeutic effects in human subjects. Our upcoming follow-up study will address these limitations by conducting clinical trials with human samples, providing a more comprehensive understanding of the practical implications.

Conclusion

Overall, the current study demonstrated that the assertion that Sox9^{+}AEC2 cells, as bona fide lung epithelial stem cells, contributed to tissue regeneration and epithelial repair through the mediation of the PI3K/AKT pathway after CALI. Sox9 regulation may emerge as a potential therapeutic target for promoting the regeneration and repair of chemical lung injuries.

Abbreviations

AEC1	Alveolar type 1 epithelial
AEC2	Alveolar type 2 epithelial
AQP5	Aquaporin 5
BADJ	Bronchoalveolar duct junction
CALI	Chemical-induced acute lung injury
DAPI	4′,6-Diamidino-2-phenylindole
EdU	5-Ethynyl-2′-deoxyuridine
ELISA	Enzyme-linked immunosorbent assay
FACS	Fluorescence assisted cell sorting
MPO	Myeloperoxidase
PBS	Phosphate-buffered saline
SOX9	Sex-determining region Y box 9
WT	Wild type

Supplementary Information

The online version contains supplementary material available at https://doi.org/10.1186/s13287-024-04124-1.

Additional file 1.

Additional file 2.

Additional file 3.

Additional file 4.

Additional file 5.

Additional file 6.

Additional file 7.

Availiability of data materials

All relevant data are included in the manuscript and supplementary material.

Declarations

Ethics approval

All animal experiments for this study were in accordance with the Animal Research: Reporting of In Vivo Experiments (ARRIVE) guidelines 2.0. All animal procedures and protocols were approved by the Institutional Animal Care and Use Committee of Jinshan Hospital, Fudan University, China (approval number: 2022-JS-008; date of approval: March 1, 2022; title of approved project: "PTTG1 mediates CD34$^+$CD45$^+$ cells to promote repair of phosgene-induced acute lung injury").

Consent for publication

All authors provided consent for publication.

Competing interests

The authors declare no competing interests.

Author details

[1]Center of Emergency and Critical Medicine, Jinshan Hospital of Fudan University, Shanghai, People's Republic of China. [2]Research Center for Chemical Injury, Emergency and Critical Medicine of Fudan University, Shanghai 201508, China. [3]Key Laboratory of Chemical Injury, Emergency and Critical Medicine of Shanghai Municipal Health Commission, Shanghai 201508, China. [4]Department of Pulmonary and Critical Care Medicine, Shanghai Respiratory Research Institute, Zhongshan Hospital, Fudan University, Shanghai 200032, China. [5]Shanghai Key Laboratory of Lung Inflammation and Injury, Shanghai 200032, China. [6]Fudan University Shanghai Medical College, Shanghai 200120, China.

References

1. Pauluhn J. Phosgene inhalation toxicity: update on mechanisms and mechanism-based treatment strategies. Toxicology. 2020;450:152682.
2. Li W, Pauluhn J. Phosgene-induced acute lung injury (ALI): differences from chlorine-induced ALI and attempts to translate toxicology to clinical medicine. Clin Transl Med. 2017;6:19.
3. Voßnacker P, Wüst A, Keilhack T, Müller C, Steinhauer S, Beckers H, et al. Novel synthetic pathway for the production of phosgene. Sci Adv. 2021;7:eabj5186.
4. Chen L, Wu D, Yoon J. Recent advances in the development of chromophore-based chemosensors for nerve agents and phosgene. ACS Sens. 2018;3:27–43.
5. Pusateri AE, Homer MJ, Rasmussen TE, Kupferer KR, Hoots WK. The interagency strategic plan for research and development of blood products and related technologies for trauma care and emergency preparedness 2015–2020. Am J Disaster Med. 2018;13:181–94.
6. Hogan BL, Barkauskas CE, Chapman HA, Epstein JA, Jain R, Hsia CC, et al. Repair and regeneration of the respiratory system: complexity, plasticity, and mechanisms of lung stem cell function. Cell Stem Cell. 2014;15:123–38.
7. Han S, Budinger GRS, Gottardi CJ. Alveolar epithelial regeneration in the aging lung. J Clin Invest. 2023;133:e170504.
8. Barkauskas CE, Cronce MJ, Rackley CR, Bowie EJ, Keene DR, Stripp BR, et al. Type 2 alveolar cells are stem cells in adult lung. J Clin Invest. 2013;123:3025–36.
9. Rock JR, Hogan BL. Epithelial progenitor cells in lung development, maintenance, repair, and disease. Annu Rev Cell Dev Biol. 2011;27:493–512.
10. Liu Q, Liu K, Cui G, Huang X, Yao S, Guo W, et al. Lung regeneration by multipotent stem cells residing at the bronchioalveolar-duct junction. Nat Genet. 2019;51:728–38.
11. Croft B, Ohnesorg T, Hewitt J, Bowles J, Quinn A, Tan J, et al. Human sex reversal is caused by duplication or deletion of core enhancers upstream of SOX9. Nat Commun. 2018;9:5319.
12. Cox JJ, Willatt L, Homfray T, Woods CG. A SOX9 duplication and familial 46, XX developmental testicular disorder. N Engl J Med. 2011;364:91–3.
13. Rockich BE, Hrycaj SM, Shih HP, Nagy MS, Ferguson MA, Kopp JL, et al. Sox9 plays multiple roles in the lung epithelium during branching morphogenesis. Proc Natl Acad Sci USA. 2013;110:E4456-4464.
14. Ma Q, Ma Y, Dai X, Ren T, Fu Y, Liu W, et al. Regeneration of functional alveoli by adult human SOX9+ airway basal cell transplantation. Protein Cell. 2018;9:267–82.
15. Sun D, Llora Batlle O, van den Ameele J, Thomas JC, He P, Lim K, et al. SOX9 maintains human foetal lung tip progenitor state by enhancing WNT and RTK signalling. EMBO J. 2022;41:e111338.
16. Laughney AM, Hu J, Campbell NR, Bakhoum SF, Setty M, Lavallée VP, et al. Regenerative lineages and immune-mediated pruning in lung cancer metastasis. Nat Med. 2020;26:259–69.
17. Cao C, Memete O, Shao Y, Zhang L, Liu F, Dun Y, et al. Single-cell RNA-sequencing reveals epithelial cell signature of multiple subtypes in chemically induced acute lung injury. Int J Mol Sci. 2022;24:277.
18. Vaughan AE, Brumwell AN, Xi Y, Gotts JE, Brownfield DG, Treutlein B, et al. Lineage-negative progenitors mobilize to regenerate lung epithelium after major injury. Nature. 2015;517:621–5.
19. Cheng KT, Xiong S, Ye Z, Hong Z, Di A, Tsang KM, et al. Caspase-11-mediated endothelial pyroptosis underlies endotoxemia-induced lung injury. J Clin Invest. 2017;127:4124–35.
20. Dun Y, Hu H, Liu F, Shao Y, He D, Zhang L, et al. PTTG1 promotes CD34+CD45+ cells to repair the pulmonary vascular barrier via activating the VEGF-bFGF/PI3K/AKT/eNOS signaling pathway in rats with phosgene-induced acute lung injury. Biomed Pharmacother. 2023;162:114654.
21. Zhang L, Zhang F, He DK, Fan XM, Shen J. MicroRNA-21 is upregulated during intestinal barrier dysfunction induced by ischemia reperfusion. Kaohsiung J Med Sci. 2018;34:556–63.
22. Gajjala PR, Kasam RK, Soundararajan D, Sinner D, Huang SK, Jegga AG, et al. Dysregulated overexpression of Sox9 induces fibroblast activation in pulmonary fibrosis. JCI Insight. 2021;6:e152503.
23. Wu J, Song D, Li Z, Guo B, Xiao Y, Liu W, et al. Immunity-and-matrix-regulatory cells derived from human embryonic stem cells safely and effectively treat mouse lung injury and fibrosis. Cell Res. 2020;30:794–809.
24. Cao C, Zhang L, Shen J. Phosgene-Induced acute lung injury: approaches for mechanism-based treatment strategies. Front Immunol. 2022;13:917395.
25. Bacakova L, Zarubova J, Travnickova M, Musilkova J, Pajorova J, Slepicka P, et al. Stem cells: their source, potency and use in regenerative therapies with focus on adipose-derived stem cells—a review. Biotechnol Adv. 2018;36:1111–26.
26. Canals I, Ginisty A, Quist E, Timmerman R, Fritze J, Miskinyte G, et al. Rapid and efficient induction of functional astrocytes from human pluripotent stem cells. Nat Methods. 2018;15:693–6.
27. Yang Y, Gomez N, Infarinato N, Adam RC, Sribour M, Baek I, et al. The pioneer factor SOX9 competes for epigenetic factors to switch stem cell fates. Nat Cell Biol. 2023;25:1185–95.
28. Ma L, Zhang R, Li D, Qiao T, Guo X. Fluoride regulates chondrocyte proliferation and autophagy via PI3K/AKT/mTOR signaling pathway. Chem Biol Interact. 2021;349:109659.
29. Li L, Feng J, Zhao S, Rong Z, Lin Y. SOX9 inactivation affects the proliferation and differentiation of human lung organoids. Stem Cell Res Ther. 2021;12:343.
30. Yang X, Liang R, Liu C, Liu JA, Cheung MPL, Liu X, et al. SOX9 is a dose-dependent metastatic fate determinant in melanoma. J Exp Clin Cancer Res. 2019;38:17.
31. Vidal VP, Chaboissier MC, Lützkendorf S, Cotsarelis G, Mill P, Hui CC, et al. Sox9 is essential for outer root sheath differentiation and the formation of the hair stem cell compartment. Curr Biol. 2005;15:1340–51.
32. Danopoulos S, Alonso I, Thornton ME, Grubbs BH, Bellusci S, Warburton D, et al. Human lung branching morphogenesis is orchestrated by the spatiotemporal distribution of ACTA2, SOX2, and SOX9. Am J Physiol Lung Cell Mol Physiol. 2018;314:L144–9.

33. Perl AK, Kist R, Shan Z, Scherer G, Whitsett JA. Normal lung development and function after Sox9 inactivation in the respiratory epithelium. Genesis. 2005;41:23–32.
34. Lim K, Donovan APA, Tang W, Sun D, He P, Pett JP, et al. Organoid modeling of human fetal lung alveolar development reveals mechanisms of cell fate patterning and neonatal respiratory disease. Cell Stem Cell. 2023;30:20-37.e9.
35. Alysandratos KD, Herriges MJ, Kotton DN. Epithelial stem and progenitor cells in lung repair and regeneration. Annu Rev Physiol. 2021;83:529–50.
36. Dye BR, Hill DR, Ferguson MA, Tsai YH, Nagy MS, Dyal R, et al. In vitro generation of human pluripotent stem cell derived lung organoids. Elife. 2015;4:e05098.
37. Fu X, Liu G, Halim A, Ju Y, Luo Q, Song AG. Mesenchymal stem cell migration and tissue repair. Cells. 2019;8:784.
38. Kucia M, Reca R, Jala VR, Dawn B, Ratajczak J, Ratajczak MZ. Bone marrow as a home of heterogenous populations of nonhematopoietic stem cells. Leukemia. 2005;19:1118–27.
39. Kadaja M, Keyes BE, Lin M, Pasolli HA, Genander M, Polak L, et al. SOX9: a stem cell transcriptional regulator of secreted niche signaling factors. Genes Dev. 2014;28:328–41.
40. Chen Q, Weng K, Lin M, Jiang M, Fang Y, Chung SSW, et al. SOX9 Modulates the transformation of gastric stem cells through biased symmetric cell division. Gastroenterology. 2023;164:1119-1136.e12.
41. Nie H, Zhao Z, Zhou D, Li D, Wang Y, Ma Y, et al. Activated SOX9+ renal epithelial cells promote kidney repair through secreting factors. Cell Prolif. 2023;56:e13394.
42. Yu L, Wei J, Liu P. Attacking the PI3K/Akt/mTOR signaling pathway for targeted therapeutic treatment in human cancer. Semin Cancer Biol. 2022;85:69–94.
43. He Y, Sun MM, Zhang GG, Yang J, Chen KS, Xu WW, et al. Targeting PI3K/Akt signal transduction for cancer therapy. Signal Transduct Target Ther. 2021;6:425.
44. Huang TT, Lampert EJ, Coots C, Lee JM. Targeting the PI3K pathway and DNA damage response as a therapeutic strategy in ovarian cancer. Cancer Treat Rev. 2020;86:102021.
45. Pons-Tostivint E, Thibault B, Guillermet-Guibert J. Targeting PI3K signaling in combination cancer therapy. Trends Cancer. 2017;3:454–69.
46. Wang H, Wang G, Meng Y, Liu Y, Yao X, Feng C. Modified Guo-Min decoction ameliorates PM2.5-induced lung injury by inhibition of PI3K-AKT and MAPK signaling pathways. Phytomedicine. 2023;123:155211.
47. Chen S, Li K, Zhong X, Wang G, Wang X, Cheng M, et al. Sox9-expressing cells promote regeneration after radiation-induced lung injury via the PI3K/AKT pathway. Stem Cell Res Ther. 2021;12:381.
48. Suryo Rahmanto A, Savov V, Brunner A, Bolin S, Weishaupt H, Malyukova A, et al. FBW7 suppression leads to SOX9 stabilization and increased malignancy in medulloblastoma. EMBO J. 2016;35:2192–212.

Publisher's Note